J|A|C|S ARTICLES

Published on Web 06/29/2010

Solution Synthesis of a New Thermoelectric $Zn_{1+x}Sb$ Nanophase and Its Structure Determination Using Automated Electron Diffraction Tomography

Christina S. Birkel,[†] Enrico Mugnaioli,[‡] Tatiana Gorelik,[‡] Ute Kolb,*[,‡] Martin Panthöfer,[†] and Wolfgang Tremel*[,†]

Institut für Anorganische Chemie und Analytische Chemie der Johannes Gutenberg-Universität, Duesbergweg 10-14, D-55099 Mainz, Germany, and Institut für Physikalische Chemie der Johannes Gutenberg-Universität, Welderweg 11, D-55099 Mainz, Germany

Received April 29, 2010; E-mail: kolb@uni-mainz.de; tremel@uni-mainz.de

Abstract: Engineering materials with specific physical properties have recently focused on the effect of nanoscopic inhomogeneities at the 10 nm scale. Such features are expected to scatter medium- and long-wavelength phonons thereby lowering the thermal conductivity of the system. Low thermal conductivity is a prerequisite for effective thermoelectric materials, and the challenge is to limit the transport of heat by phonons, without simultaneously decreasing charge transport. A solution-phase technique was devised for synthesis of thermoelectric "Zn_4Sb_3" nanocrystals as a precursor for phase segregation into ZnSb and a new Zn−Sb intermetallic phase, $Zn_{1+\delta}Sb$, in a peritectoid reaction. Our approach uses activated metal nanoparticles as precursors for the synthesis of this intermetallic compound. The small particle size of the reactants ensures minimum diffusion paths, low activation barriers, and low reaction temperatures, thereby eliminating solid−solid diffusion as the rate-limiting step in conventional bulk-scale solid-state synthesis. Both phases were identified and structurally characterized by automated electron diffraction tomography combined with precession electron diffraction. An ab initio structure solution based on electron diffraction data revealed two different phases. The new pseudo-hexagonal phase, $Zn_{1+\delta}Sb$, was identified and classified within the structural diversity of the Zn−Sb phase diagram.

Introduction

Thermoelectric materials allow the conversion of a thermal gradient into a gradient of the electrical potential and may play a vital role in the search for alternative energy technologies.[1,2] The thermoelectric performance of a material is expressed by a dimensionless figure of merit, $ZT = S^2T/\rho\kappa$, where S is the thermopower; ρ is the electrical resistivity; κ is the thermal conductivity; and T is the temperature. Heat is carried by both electrons (κ_e) and phonons (κ_{ph}),[3] thus the total thermal conductivity is the sum of the lattice thermal conductivity and the electronic thermal conductivity. While the latter can be estimated from the electrical conductivity using the Wiedemann−Franz law,[6] the lattice thermal conductivity is closely related to the crystal structure.

Among thermoelectric materials, "Zn_4Sb_3" (more precisely $Zn_{3.9-x}Sb_3$) exhibits an outstanding figure of merit between 450 and 670 K with $ZT \approx 1.3$ at 670 K, owing to its exceptionally low thermal conductivity.[4,5] Structure and precise stoichiometry of "Zn_4Sb_3" have been studied for decades.[5,6,7,8−16] Common to all four known phases in the phase diagram is a framework of isolated Sb^{3-} anions and Sb_2^{4-} dumbbells, the latter being centered in a metaprism formed by six Zn cations. Apart from the high-temperature γ-phase, all low-temperature phases exhibit occupational disorder in the Zn partial structure and occupation of interstitials with decreasing level of order upon decreasing

[†] Institut für Anorganische Chemie und Analytische Chemie der Johannes Gutenberg-Universität.

[‡] Institut für Physikalische Chemie der Johannes Gutenberg-Universität.

(1) Goldsmid, H. J. *Thermoelectric Refrigeration*; Plenum Press: New York, 1988.
(2) Wood, C. *Rep. Prog. Phys.* **1988**, *51*, 459–539.
(3) Ziman, J. M. *Prinzipien der Festkörpertheorie*; Verlag Harry Deutsch: Zürich und Frankfurt am Main, 1972.
(4) Bhattacharya, S.; Hermann, R. P.; Keppens, V.; Tritt, T. M.; Snyder, G. J. *Phys. Rev. B* **2006**, *74*, 134108.
(5) Caillat, T.; Fleurial, J. P.; Borshchevsky, A. *J. Phys. Chem. Solids* **1997**, *58*, 1119–1125.
(6) Elliott, S. *The Physics and Chemistry of Solids*; Wiley and Sons: Chichester, 1998.
(7) Kim, S. G.; Mazin, I. I.; Singh, D. J. *Phys. Rev. B* **1998**, *57*, 6199–6203.
(8) Mayer, H. W.; Mikhail, I.; Schubert, K. *J. Less-Common Met.* **1978**, *59*, 43–52.
(9) Snyder, G. J.; Christensen, M.; Nishibori, E.; Caillat, T.; Iversen, B. B. *Nat. Mater.* **2004**, *3*, 458–463.
(10) Cargnoni, F.; Nishibori, E.; Rabiller, P.; Bertini, L.; Snyder, G. J.; Christensen, M.; Gatti, C.; Iversen, B. B. *Chem.−Eur. J.* **2004**, *10*, 3862–3870.
(11) Mozharivskyj, Y.; Pecharsky, A. O.; Bud'ko, S.; Miller, G. J. *Chem. Mater.* **2004**, *16*, 1580–1589.
(12) Nylen, J.; Andersson, M.; Lidin, S.; Häussermann, U. *J. Am. Chem. Soc.* **2004**, *126*, 16306–16307.
(13) Mozharivskyj, Y.; Janssen, Y.; Harringa, J. L.; Kracher, A.; Tsokol, A. O.; Miller, G. J. *Chem. Mater.* **2006**, *18*, 822–831.
(14) Nylen, J.; Lidin, S.; Andersson, M.; Iversen, B. B.; Liu, H.; Newman, N.; Häussermann, U. *Chem. Mater.* **2007**, *19*, 834–838.
(15) Nylen, J.; Lidin, S.; Andersson, M.; Liu, H.; Newman, N.; Häussermann, U. *J. Solid State Chem.* **2007**, *180*, 2603–2615.
(16) Schweika, W.; Hermann, R. P.; Prager, M.; Persson, J.; Keppens, V. *Phys. Rev. Lett.* **2007**, *99*, 125501.

temperature. The amount of occupation of interstitials seems to be sample dependent, thus "Zn_4Sb_3" has become a generic term for the group of structurally comparable compounds $Zn_{6-\delta}Sb_5$ ($\delta = 0.62, 0.76$),[13] $Zn_{3.83}Sb_3$,[14] and $Zn_{84}Sb_{65}$.[15]

The proposed structures are variants of a Zn_6Sb_5 basis structure with structural disorder due to additional Zn interstitials and Zn vacancies[9–12,14] and have been derived from comprehensive X-ray diffraction studies and analyses using maximum entropy methods. Recent inelastic neutron scattering investigations relate low thermal conductivity not to a phonon glass but to a soft localized vibration of dumbbell Sb_2 units in the Sb sublattice.[4,16]

The interdependency of transport properties in *ZT* makes the engineering of thermoelectric materials a difficult task. However, the physics of nanostructures allows varying S, ρ, and κ independently, thus enhancing *ZT* under appropriately selected conditions. The greatest gains in *ZT* have been achieved by introducing interfaces such that phonons are preferentially scattered relative to electrons. Different approaches to decrease κ_{ph} by reducing the mean free path of phonons while maintaining the electronic properties of doped semiconductors have been attempted: (i) alloying,[17] (ii) nanostructuring,[18,19] and (iii) guest atom inclusion.[20,21] Prominent examples of thermoelectric materials based on the "phonon glass-electron crystal" concept[22,23] are the skutterudites[22] or "Zn_4Sb_3" studied here.

One strategy for creating the required scattering interfaces relies on the synthesis of nanoparticles and multiphase composites mixed on the nanometer scale. These nanostructured materials can be formed as thin-film superlattices or as intimately mixed composite structures. The first demonstration that a low-dimensional material system could enhance thermoelectric performance was for a 2D superlattice consisting of PbTe quantum wells, $Pb_{1-x}Eu_xTe$ barriers,[24] and $(Bi,Sb)_2Te_3$ superlattices.[25,26] Epitaxial-type superlattice structures are formed, and their sizes can be controlled by phase separation of metastable ternary compounds into their corresponding binaries.[19,20,27,28]

The following question thus arises: can we conceive other materials, based on solidification and decomposition, which may lead to enhanced *ZT*-values? Here, we present an extension of the "solidification and decomposition" approach to thermoelectric materials at the nanoscale using thermolabile "Zn_4Sb_3" as the starting compound.

From a synthetic point of view, it is crucial to control the nanostructure and morphology of these complex binary materials and their performance in potential thermoelectric applications. Controlling nanostructure and morphology is important, as they are critical for the intended applications. Intermetallics are typically made at high temperatures (usually >1000 °C) with long annealing times (often days or weeks). Due to the intrinsically metastable nature of nanoscale matter, we have devised a low-temperature synthetic route for "Zn_4Sb_3" nanoparticles, where weakly stabilized Zn and Sb nanoparticles aggregate to form binary nanocomposites[29] reacting subsequently to form intermetallic nanocrystals. The synthesis can be scaled up to yield bulk amounts of material. The novel solution-based approach uses activated metal nanoparticles as precursors for the synthesis of a $Zn_{1+x}Sb$ nanophase, containing ZnSb and a new binary phase $Zn_{1+\delta}Sb$, segregated from a nano-Zn_4Sb_3 precursor in a peritectoid reaction.

Traditional single-crystal X-ray diffraction techniques cannot be applied to nanostructures. Powder X-ray analysis meets serious problems when the size of the crystals is below 50 nm and different phases are present in the sample, all attributes of the Zn−Sb system. Therefore, the crystallographic investigation was performed using electron diffraction. In contrast to X-rays, an electron beam can be focused on a very small area allowing the selection of a single nanocrystal of only a few nanometers. As scattering factors for electrons are significantly higher in comparison to X-rays, diffraction information with a reasonable signal-to-noise ratio can be collected even from such small volumes. Two types of problems are usually attributed to electron diffraction data, which diminishes its usability for structure solution: electron diffraction data often miss a sufficient number of reflections, and the intensities of the reflections are strongly modified due to dynamical effects. To overcome these problems and to develop a well-established routine for electron diffraction data collection, techniques like automated diffraction tomography (ADT)[30,31] and precession electron diffraction (PED)[32−34] have been developed in the last years. By combining these two techniques, a rich sampling of the reciprocal space can be achieved, and thus almost complete quasi-kinematical electron diffraction data sets can be collected. Mugnaioli et al.[35] demonstrated that this method, comprising basically the 3D reconstruction of the reciprocal space with quasi-kinematical data, allows solving inorganic structures ab initio in one step. This data collection/structure solution strategy was applied to the $Zn_{1+x}Sb$ nanophase containing a known ZnSb phase and a hitherto unknown $Zn_{1+\delta}Sb$. Both phases were identified by electron diffraction and high-resolution TEM imaging, and ab initio structure determinations were performed using combined ADT/PED.

Results and Discussion

Synthesis. Synthesis of the $Zn_{1+x}Sb$ nanophase was achieved through the reaction of "activated" zinc with "activated"

(17) Kimura, Y.; Zama, A. *Appl. Phys. Lett.* **2006**, *89*, 103705.
(18) Hsu, K. F.; Loo, S.; Guo, F.; Chen, W.; Dyck, J. S.; Uher, C.; Hogan, T. P.; Polychroniadis, E. K.; Kanatzidis, M. G. *Science* **2004**, *303*, 818–821.
(19) Poudeu, P. F. R.; D'Angelo, J.; Downey, A. D.; Short, J. L.; Hogan, T. P.; Kanatzidis, M. G. *Angew. Chem.* **2006**, *118*, 3919−3923; *Angew. Chem., Int. Ed.* **2006**, *45*, 3835−3839.
(20) Nolas, G. S.; Cohn, J. L.; Slack, G. A.; Schujman, S. B. *Appl. Phys. Lett.* **1998**, *73*, 178–180.
(21) Keppens, V.; Mandrus, D.; Sales, B. C.; Chakoumakos, B. C.; Dai, P.; Coldea, R.; Maple, M. B.; Gajewski, D. A.; Freeman, E. J.; Bennington, S. *Nature* **1998**, *395*, 876–878.
(22) Sales, B. C.; Mandrus, D.; Williams, R. K. *Science* **1996**, *272*, 1325–1328.
(23) Nolas, G. S.; Morelli, D. T.; Tritt, T. M. *Annu. Rev. Mater. Sci.* **1999**, *29*, 89–116.
(24) Hicks, L. D.; Harman, T. C.; Sun, X.; Dresselhaus, M. S. *Phys. Rev. B* **1996**, *53*, R10493.
(25) Martin-Gonzalez, M.; Snyder, G. J.; Prieto, A. L.; Gronsky, R.; Sands, T.; Stacy, A. M. *Nano Lett.* **2003**, *3*, 973–977.
(26) Caylor, J. C.; Coonley, K.; Stuart, J.; Colpitts, T.; Venkatasubramanian, R. *Appl. Phys. Lett.* **2005**, *87*, 023105.
(27) Ikeda, T.; Ravi, V. A.; Snyder, G. J. *J. Mater. Res.* **2008**, *9*, 2538–2546.
(28) Ikeda, T.; Collins, L. A.; Ravi, V. A.; Gascoin, F. S.; Haile, S. M.; Snyder, G. J. *Chem. Mater.* **2007**, *19*, 763–767.
(29) Schlecht, S.; Erk, C.; Yosef, M. *Inorg. Chem.* **2006**, *45*, 1693–1697.
(30) Kolb, U.; Gorelik, T.; Kubel, C.; Otten, M. T.; Hubert, D. *Ultramicroscopy* **2007**, *107*, 507–513.
(31) Kolb, U.; Gorelik, T.; Otten, M. T. *Ultramicroscopy* **2008**, *108*, 763–772.
(32) Vincent, R.; Midgley, P. A. *Ultramicroscopy* **1994**, *53*, 271–282.
(33) Own, C. S. System Design and Verification of the Precession Electron Diffraction Technique, Ph.D. dissertation, Northwestern University, 2005.
(34) Avilov, A.; Kuligin, K.; Nicolopoulos, S.; Nickolskiy, M.; Boulahya, K.; Portillo, J.; Lepeshov, G.; Sobolev, B.; Collette, J. P.; Martin, N.; Robins, A. C.; Fischione, P. *Ultramicroscopy* **2007**, *107*, 431–444.

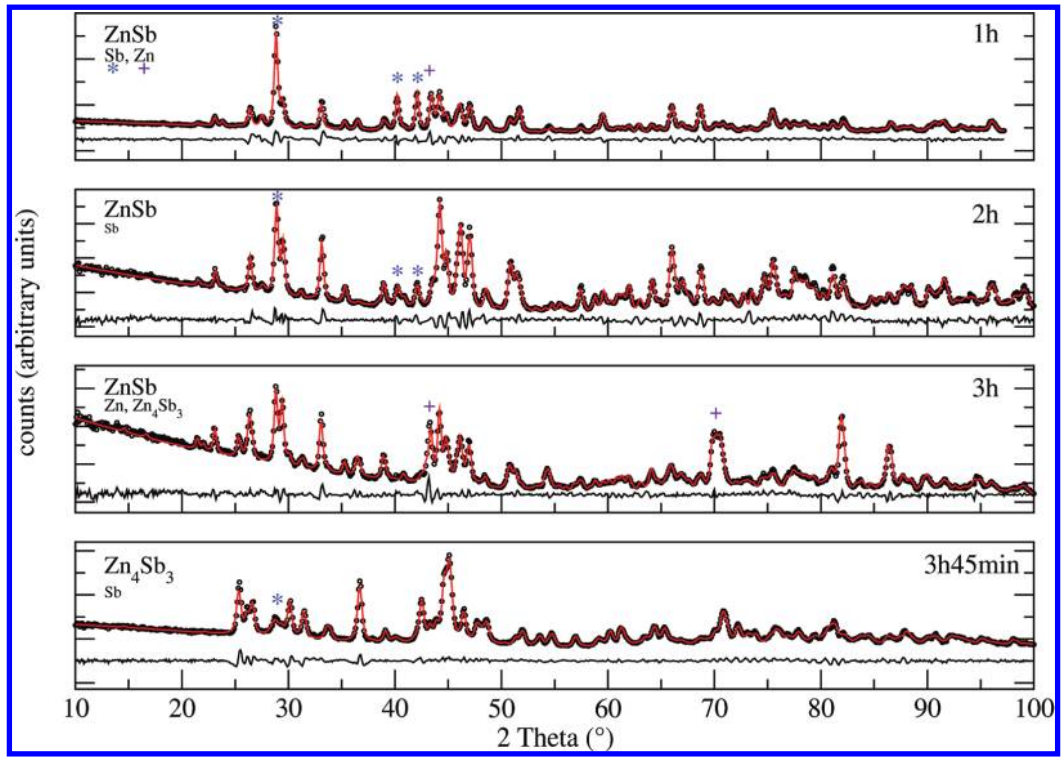

Figure 1. Time-dependent (ex situ) X-ray diffraction (experimental data: black circles), le Bail fits (red line), and corresponding difference plots (black line) after reaction times of 60, 120, 180 (as prepared), and 225 min (after two washing cycles with dilute acetic acid).

antimony in the temperature range of 275−300 °C. "Activated" reactants were produced by reduction of $ZnCl_2$ and $SbCl_3$ with lithium triethylboronhydride $Li[Et_3BH]$ at 65 °C in tetrahydrofuran. The black metal powders obtained were redispersed repeatedly in dry tetrahydrofuran to remove residual lithium salts and were subsequently dried in vacuo. Both Zn and Sb nanoparticles are highly reactive in ambient air leading primarily to the oxides. ^{1}H NMR data of Sb nanoparticles kept in an inert gas atmosphere show an intense signal according to surface bond stibane ($\delta \approx 1.05$ ppm, c.f. Figure SI-1, Supporting Information) which broadens when the particles are in contact with air.

The activated elements were heated to 300 °C at a rate of ca. 20 K/min in a polar strongly coordinating solvent (trioctylamine) to prevent nanoparticle aggregation. Products were collected by centrifugation, washed with ethanol, and subsequently dried in vacuo. The syntheses had to be carried out using an excess of zinc metal which is removed after reaction by repeated treatment of the solid residue with dilute acetic acid. Prior to heating, both Zn and Sb were crystalline, and the XRD pattern matched that expected for a superposition of both elements. After several minutes of heating at 300 °C, the intermetallic compound ZnSb was formed; further heating increased its crystallinity. The product is stable in air at least over the period of several months.

Combined TG/DTA of the product in the range from ambient temperature to 450 °C showed an exothermic effect at 200 °C corresponding to the peritectoid decomposition of $Zn_{1+x}Sb$, forming ZnSb and Zn. Upon further heating, the melting of Zn (ca. 410 °C) was observed, while only a minor weight loss occurred.

It was observed that the size of an activated metal particle is crucial for the outcome of the reaction. In conventional high-temperature reactions, the energy required for the solid state diffusion of the reactants would exceed the nucleation energy of metastable phases. In contrast, reactions, in which solid state diffusion plays only a minor role, are kinetically controlled, and a phase may nucleate and grow until its growth exhausts the supply of the reactants. The sequence of phases formed depends upon the relative activation energies for nucleation of the various compounds, and compounds in the equilibrium phase diagram may be temporarily skipped if they have large activation energy for nucleation. The size of the "activated" metal particles allows for a reaction with minimum solid state diffusion, low activation barriers, and low reaction temperatures, thereby eliminating solid−solid diffusion as the rate-limiting step in conventional bulk-scale solid-state synthesis. It follows the strategy proposed by Johnson et al.[36,37] on elementally modulated thin films that was utilized later for the synthesis of fullerene-type chalcogenide nanoparticles[38] or in the so-called polyol synthesis for nanoparticles of noble metals[39] and intermetallics.[40] The nanosize dimensions support low-temperature diffusion without the high-temperature melting step that is necessary in traditional metallurgy. Clearly, nanoscale intermixing of prereduced metal particles significantly increases the reaction kinetics relative to conventional high-temperature syntheses involving micrometer-sized powders. Likewise, the solvent confines the crystallite size to nanoscale dimensions, allowing atomic ordering to occur rapidly without long-term annealing.

X-ray Diffraction. X-ray powder diffraction profiles recorded from reaction intermediates after specified time intervals (Figure

(35) Mugnaioli, E.; Gorelik, T.; Kolb, U. *Ultramicroscopy* **2009**, *109*, 758–765.

(36) Novet, T.; Johnson, D. C. *J. Am. Chem. Soc.* **1991**, *113*, 3398–3403.
(37) Noh, M.; Thiel, J.; Johnson, D. C. *Science* **1995**, *270*, 1181–1184.
(38) Etzkorn, J.; Therese, H. A.; Rocker, F.; Zink, N.; Kolb, U.; Tremel, W. *Adv. Mater.* **2005**, *17*, 2372–2375.
(39) Sun, Y. G.; Xia, Y. N. *Science* **2002**, *298*, 2176–2179.
(40) Leonard, B. M.; Bhuvanesh, N. S. P.; Schaak, R. E. *J. Am. Chem. Soc.* **2005**, *127*, 7326–7327.

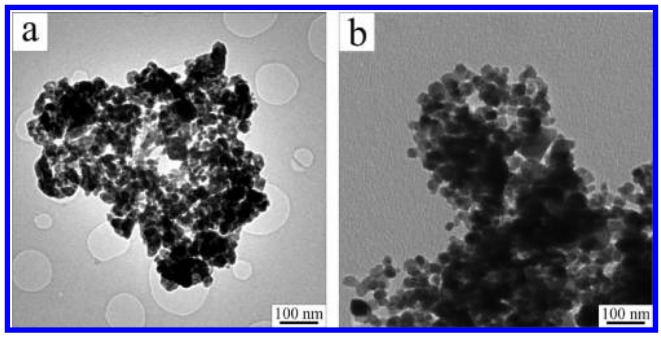

Figure 2. Overview TEM images of typical aggregates obtained after (a) a reaction time of 1 h and (b) the final product after 3 h 45 min.

1) revealed that ZnSb was formed within 1 h. From the X-ray powder data, it was evident that the primary product transformed into a new phase with cell parameters geometrically related to those of "Zn_4Sb_3" in the subsequent reaction steps. The data collected after reaction intervals of 2 and 3 h indicated the formation of a mixture of ZnSb and nominal Zn_4Sb_3, which was the major product when the reaction was complete after 3 h 45 min. Upon further heating, a reformation of ZnSb due to decomposition of Zn_4Sb_3 (mostly into Zn) was observed (Figure SI-3, Supporting Information). If the amount of Zn was less than a 9-fold excess, the major product of the reaction was ZnSb instead of Zn_4Sb_3.

All diffraction profiles included reflections of metallic Sb and Zn (marked in Figure 1 by blue stars and magenta crosses, respectively). The final product obtained after 225 min contains only minor amounts of these impurities. The powder patterns of all crystalline phases were refined using le Bail fits with lattice cell parameters of ZnSb and Zn_4Sb_3.[11] The fitting of the final product was carried out using the crystallographic data of Zn_4Sb_3 and gave an almost straight difference curve indicating that there are no further crystalline impurities. The crystallite size of the Zn_4Sb_3 nanoparticles as determined from the refinement was approximately 30 nm.

TEM Overview. In all TEM investigations, the samples proved to be extremely stable; i.e., no alteration was observed either in short-term or after hours of data acquisition. TEM images as well as SEM images show that both the intermediate and the final products consist of porous agglomerates built of tens to hundreds of round particles (Figure 2, Figure SI-4, Supporting Information) with diameters between 5 and 70 nm. The mean particle size determined from TEM is therefore in harmony with the crystallite size obtained from the powder X-ray studies. Despite intensive sonication during TEM sample preparation, individual crystals were never observed, and even the smallest aggregates consisted of several crystals (Figure 3).

HRTEM images of the final $Zn_{1+x}Sb$ nanophase demonstrated that all particles but the smallest contain a crystalline core surrounded by an amorphous shell of 3−10 nm (Figure 4, Figure SI-5, Supporting Information). Although the sample crystallinity judged from the powder X-ray profiles did not differ much for the products after different reaction times, HRTEM imaging showed that the final product (obtained after 3 h 45 min) has significantly higher crystallinity.

High-resolution TEM measurements of the final product as well as electron diffraction patterns clearly revealed the presence of a crystallographic phase different from any known Zn_4Sb_3 phase. Although powder X-ray profiles could be fitted using the crystallographic data of Zn_6Sb_5,[11] TEM delivered a pseudohexagonal lattice and interplanar distances which could not be

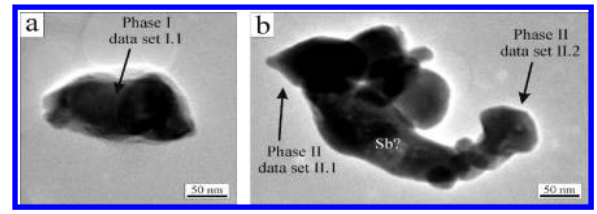

Figure 3. Small aggregates used for ADT data collections. (a) Data for structural analysis of phase I were collected from the middle part of the agglomerate. (b) Two data sets for structural analysis of phase II were collected from crystals indicated by arrows. In the middle part of this aggregate, diffraction patterns with interplanar distances of 11.2 Å were observed, likely due to the presence of metallic Sb.

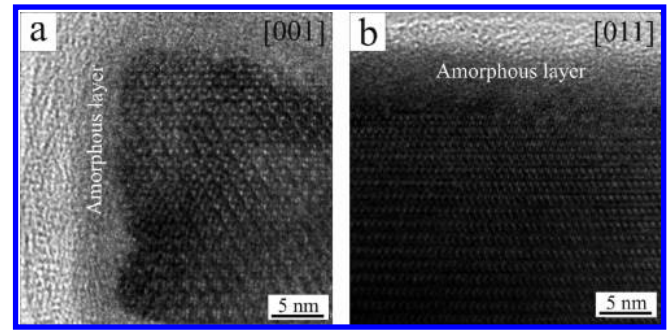

Figure 4. HRTEM images of $Zn_{1+\delta}Sb$ nanoparticles viewed along (a) the [001] and (b) the [011] directions.

described by any known phase. Obviously, the lattice parameters of the new phase should be strictly geometrically related to Zn_6Sb_5. The cell volume of the new phase, calculated by high-order Laue zones (Figure SI-5, Supporting Information), is approximately 1630 Å^3. EDX analyses of multiple regions of the samples confirm that Zn and Sb are present in an approximate 1:1 atomic ratio with a slight excess of Zn (53% Zn, 47% Sb; Figure SI-6, Supporting Information).

Electron Crystallography by ADT. For structural investigations, ADT data were collected from prominent crystals in relatively small aggregates (Figure 3) using an electron beam with 50 nm diameter (for details, see refs 30 and 31). 3D reconstruction of the reciprocal space for different crystals showed unambiguously that the sample consisted at least of two different phases. While the first phase had an orthorhombic cell (phase I), the second one showed a lattice with pseudo-hexagonal metric (phase II). Approximate average compositions determined from EDX spectra did not allow an unambiguous determination of the two phases, as for both the Sb:Zn ratio was close to 1:1.

Figure 5 shows projections of the reconstructed reciprocal volume from ADT data for orthorhombic phase I. The unit cell parameters agree well with the known structure of ZnSb (Table 1).[11] The systematic extinctions are compatible with the space group *Pbca*. Lattice parameters determined directly from ADT data, as well as subsequently refined against powder X-ray diffraction data, are approximately 4% larger than those reported for the ZnSb bulk phase.

The most important information about the ADT data set used for structure analysis of phase I is compiled in Table 2. The structure was solved ab initio in one step using direct methods implemented in SIR2008[41] from ADT data without electron beam precession (Figure SI-8, Supporting Information). A fully

(41) Sheldrick, G. M. *Acta Crystallogr., Sect. A* **2008**, *64*, 112–122.

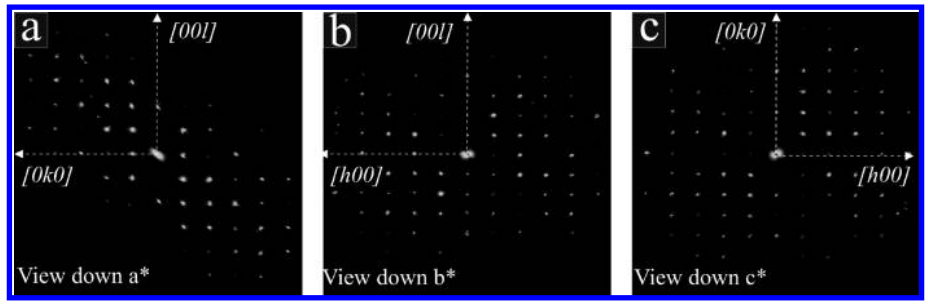

Figure 5. Projections of the full 3D reciprocal space for the orthorhombic phase I of the data set I.1 exhibiting the systematic extinctions of space group *Pbca* (see Figure SI-7, Supporting Information, and comment). The volume was visualized using the ADT-3D package applying a volume-rendering technique with manually determined opacity transfer functions.

Table 1. Crystallographic Data of the Two Different Crystalline Phases

	ZnSb			$Zn_{1+\delta}Sb$	
cell parameters	ADT	refined XRPD	11	ADT	XRPD
space group		*Pbca*		*P*-1	
a (Å)	6.46	6.54	6.20	15.31	15.25
b (Å)	8.11	8.06	7.74	15.51	15.72
c (Å)	8.43	8.31	8.10	7.81	7.81
α (°)	89.31	90	90	88.87	90
β (°)	89.86	90	90	89.42	90
γ (°)	89.38	90	90	119.4	120

Table 2. Summary of the ADT Data Sets Employed for Structure Determination

	ZnSb	$Zn_{1+\delta}Sb$	
data set	I.1	II.1	II.2
data type	ADT	ADT + PED	ADT + PED
tilt range	60°	76° + 76°	90°
total reflections	388	6271	4486
independent reflections	106	3651	2745
resolution (Å)	1.1	0.8	0.8
reflection coverage, %	70	57	44
R_{sym}, % of the data set	30.60	16.86	17.45
U isotropic (Å^2)	0.037	0.030	0.031
final *R*, %	27.10	36.19	42.52

kinematical approach was used (intensities proportional to F_{hkl}^2), and no correction was applied to the data. Four potential peaks were identified by the program. The most intense peak (the height of 1596) was assigned to an Sb atom; the second peak (the height of 910) was assigned to Zn. The ratio between the heights of these two peaks corresponds nicely to the ratio between the atomic numbers of the two atoms 51:30, which in turn reflects the maximal amplitudes of the scattering factors for electrons. The other two peaks found by SIR2008 were much lower (305 and 300) and therefore were treated as ghosts. The structure model exhibits a close match to the known crystal structure of ZnSb[11] with the errors in atomic positions of 0.02 Å for Sb and 0.05 Å for Zn.

Main projections of a 3D reconstructed data set recorded for phase II ($Zn_{1+\delta}Sb$) are shown in Figure 6a,b. The corresponding lattice parameters are listed in Table 1. ADT data confirm that the cell parameters did not match those of any known Zn−Sb phase, even if the new phase has to be strictly geometrically related with rombohedral Zn_6Sb_5.[11] No systematic extinction was detected. The lattice parameters obtained from electron diffraction allowed reasonable le Bail fitting of the powder X-ray diffraction profile, taking into account impurities of Sb and ZnSb (Table 1).

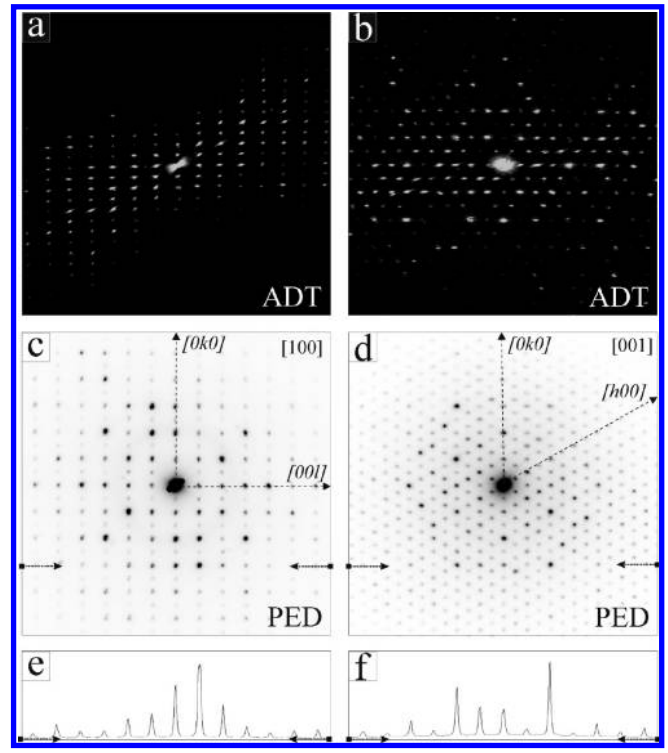

Figure 6. Electron diffraction data for phase II ($Zn_{1+\delta}Sb$): (a) projection of the reconstructed reciprocal space along the *a** direction; (b) projection of the reconstructed reciprocal space along the *c** direction; (c) single PED pattern zone [100]; (d) single PED pattern zone [001]; (e, f) intensity scans of patterns shown in (c) and (d) (line marked by arrows).

To determine the correct crystal system for phase II, single zone diffraction patterns taken at optimized electron beam precession conditions were recorded (Figure 6c,d). Both, zone [100] and zone [001] exhibit strong pseudo-symmetry. However, a careful inspection of the [100] zone shows that the only true symmetry element present is the inversion center (due to Friedel's law). Figure 6e shows an intensity scan along the row marked in Figure 6c by dotted arrows: these reflections do not have mirror symmetry along the [010] direction. The [001] zone shows no mirror symmetry (Figure 6f), and a careful analysis of prominent spots, such as, for example, (400), (040), and (−440), leads to an exclusion of a 3-fold axis. Therefore, the true zone symmetry is inversion only, and the structure is triclinic.

For structure analysis of phase II, two independent tilt series were collected. The first crystal was tilted in a range of 76°, rotated in-plane by approximately 90° and tilted again by 76° collecting an additional tilt series in the same tilt range. These

two tilt series acquired from the same crystal were subsequently merged (merging factors 1 to 1) and gave data sets II.1 (Table 2). The second data set II.2 was collected from another crystal within a tilt range of 90° (Table 2). The diffraction camera length was reduced to achieve a resolution of 0.8 Å. Both data sets include around 3000 independent reflections.

For phase II, structure solution by direct methods based on standard ADT data did not result in a chemically meaningful structure model. The ADT−PED coupled data set should be superior for structure solution;[35] therefore, as a next step these data were tried. Indeed, a first solution in space group P1 converged to a reasonable structural model in one step. A check of the atomic positions displayed immediately the presence of an inversion center in the structure. This additional symmetry element was also evident from the correlation coefficient matrix in the initial structure model refinement. Therefore the structure was finally solved in space group P-1. A fully kinematical approach was used, and no correction was applied to the data set. The correct solution was well recognizable as it exhibited by far the lowest final residual factor and the highest figure of merit at the same time. The first 30 maxima in the electron density map determined by SIR2008[41] showed reasonable interatomic distances. The 14 strongest maxima were attributed to Sb and the remaining 16 to Zn. The structure was subsequently refined using SHELXL97,[42] showing an appreciable stability without any constraints. The final refinement converges at $R = 0.362$ and 0.425 for data I and II, respectively, which is in the typical level of quality for crystal structure analysis by ADT and electron diffraction in general.[35] As the Zn_4Sb_3 compounds are known to exhibit occupational disorder of the Zn partial structure, the atomic occupancies for all atoms were tentatively refined based on the available electron diffraction data. Even if the reliability of site occupation factors derived from electron diffraction data is a subject of discussion, values significantly lower than 1 are usually taken as a hint toward occupational disorder.[43] Taking into account the partial occupancies, the final stoichiometry of the $Zn_{1+\delta}Sb$ phase is $Zn_{28.1}Sb_{26.3}$.

A full occupancy of the positions results in a density of 5.63 g/cm^3, which is in good agreement with the density of 5.68 g/cm^3 calculated for the orthorhombic ZnSb phase. If the refined occupancies are taken into account, the density drops to 5.10 g/cm^3. A possible explanation is that the vacancies are partially compensated by interstitials as often found for such compounds.[11] Final residual electron density maps still displayed intermediate to weak maxima which point to further Zn positions. Yet, within the given level of detail of electron diffraction an expansion of the structure model, taking these maxima into account, would not be appropriate. Albeit the occupational disorder of the Zn partial substructure, the isotropic displacement factors were refined stable and exhibited reasonable values (Table SI-2, Supporting Information).

To confirm the above model, the second ADT+PED data set II.2 was analyzed using the same routine. The result confirms the structure model described above. The maximal difference of the atomic positions was 0.41 Å, and the average difference was 0.18 Å.

Crystal Structure of $Zn_{1+\delta}Sb$. Projections of the crystal structure are presented and compared with $Zn_{13}Sb_{10}$[13] in Figure 7. Single zone diffraction patterns of phase II (Figure 5c and d) show a strong superstructure imprint with hexagonal symmetry. In fact, the Sb substructure displays 6/*m* symmetry with all Sb placed on special positions according to the 2*e*, 2*d*, 6*i*, 6*j*, 6*j*, 6*k* Wyckoff sites of space group P6/*m*. The Zn substructure reduces the symmetry of the complete structure to −1. Yet, parts of the Zn substructure exhibit some higher symmetry: i.e., some of the nonsymmetry equivalent coordination polyhedra are very similar. For example, the polyhedrons in the middle row arranged along [010] show very similar organization (cf. Figure 7a). This result is quite impressive as no specific symmetry constraints were imposed during the structure model refinement.

The structure can be classified within the Zintl−Klemm concept.[44−46] Antimony being more electronegative than Zn forms two types of anions: isolated Sb^{3-} anions and $(Sb_2)^{4-}$ dumbbells (molecule-anions). The Sb^{3-} anions (Sb1, Sb2, Sb3, and Sb7) in $Zn_{1+\delta}Sb$ form a flat hexagonal net at $z = 1/2$ with the distances of 4.4−4.6 Å between the nodes (Figure 8a). This net is placed at 1/2 height of the unit cell (in [001] direction). The remaining Sb species belong to two different kinds of $(Sb_2)^{4-}$ dumbbells. The first ones are those aligned in [001] direction and placed with the centers of gravity at virtually the same height as the hexagonal net (Figure 8b). These antimony species are located at four corners of the unit cell (Sb9), at four faces (Sb6, Sb8), and in the center (Sb10). In total, there are four $(Sb_2)^{4-}$ dumbbells of this kind (Figure b). The second type of dumbbells (Sb4, Sb5, Sb11, Sb12, Sb13, Sb14) is placed at the $z = 0$ and is aligned within the (001) plane in a windmill pattern (Figure 8c).

Several crystalline phases are known within the Zn−Sb phase diagram close to the 1:1 composition: orthorhombic ZnSb (*Pbca*), $Zn_{13}Sb_{10}$ (three polymorphs crystallizing in space groups *R*-3*c*, *C*2/*c*, and *C*-1 (11)), and α- and β-Zn_4Sb_3.[14,15] The structure of $Zn_{1+\delta}Sb$ is very closely related to the rhombohedral polymorph of $Zn_{13}Sb_{10}$: both display a hexagonally packed channel structure. This similarity is seen the best in [001] projections (Figure 7a and b). The lattice parameters *a* and *b* are connected by the transformation sketched in Figure 7: $a_{P\text{-}1} = 2/3 \times (a_{R3c} - b_{R3c})$, $b_{P\text{-}1} = 2/3 \times (a_{R3c} + 2b_{R3c})$. Yet, the two structures look very different when viewed from the side (Figure 7c and d). In the rhombohedral polymorph of $Zn_{13}Sb_{10}$, the Sb_2^{4-} dumbbells are shifted up and down along [001], while the Sb_2^{4-} dumbbells in $Zn_{1+\delta}Sb$ are located on the same height. The orthorhombic ZnSb, in turn, has a more complicated arrangement consisting of three independent intercalating sets of Sb_2^{4-} dumbbells.

In contrast to the rhombohedral polymorph of $Zn_{13}Sb_{10}$, in which each Sb atom of a dumbbell is coordinated by three Zn atoms, the Sb atoms in Zn_8Sb_7 are coordinated by four Zn atoms (compare Figure 7c and d). This coordination of Sb is, in turn, consistent with the coordination observed in ZnSb.

The distances between Sb atoms within the dumbbells range from 2.72 to 2.91 Å and are in a good agreement with the corresponding distances for the *R*-3*c* $Zn_{13}Sb_{10}$ structure and for orthorhombic ZnSb. The distances between the Sb in the dumbbells and the coordinating Zn also agree well with the

(42) Burla, M. C.; Caliandro, R.; Camalli, M.; Carozzini, B.; Cascarano, G. L.; De Caro, L.; Giacovazzo, C.; Polidori, G.; Siliqi, D.; Spagna, R. *J. Appl. Cryst.* **2007**, *40*, 609−613.
(43) Jansen, J. *Structure Refinement by Taking Dynamical Diffraction into Account*; Springer: Netherlands, 2006.
(44) Zintl, E. *Angew. Chem.* **1939**, *52*, 1–6.
(45) Nesper, R. *Angew. Chem.* **1991**, *103*, 805−834; *Angew. Chem., Int. Ed.* **1991**, *30*, 789−817.
(46) Papoian, G. A.; Hoffmann, R. *Angew. Chem.* **2000**, *112*, 2500−2544; *Angew. Chem., Int. Ed.* **2000**, *39*, 2409−2448.

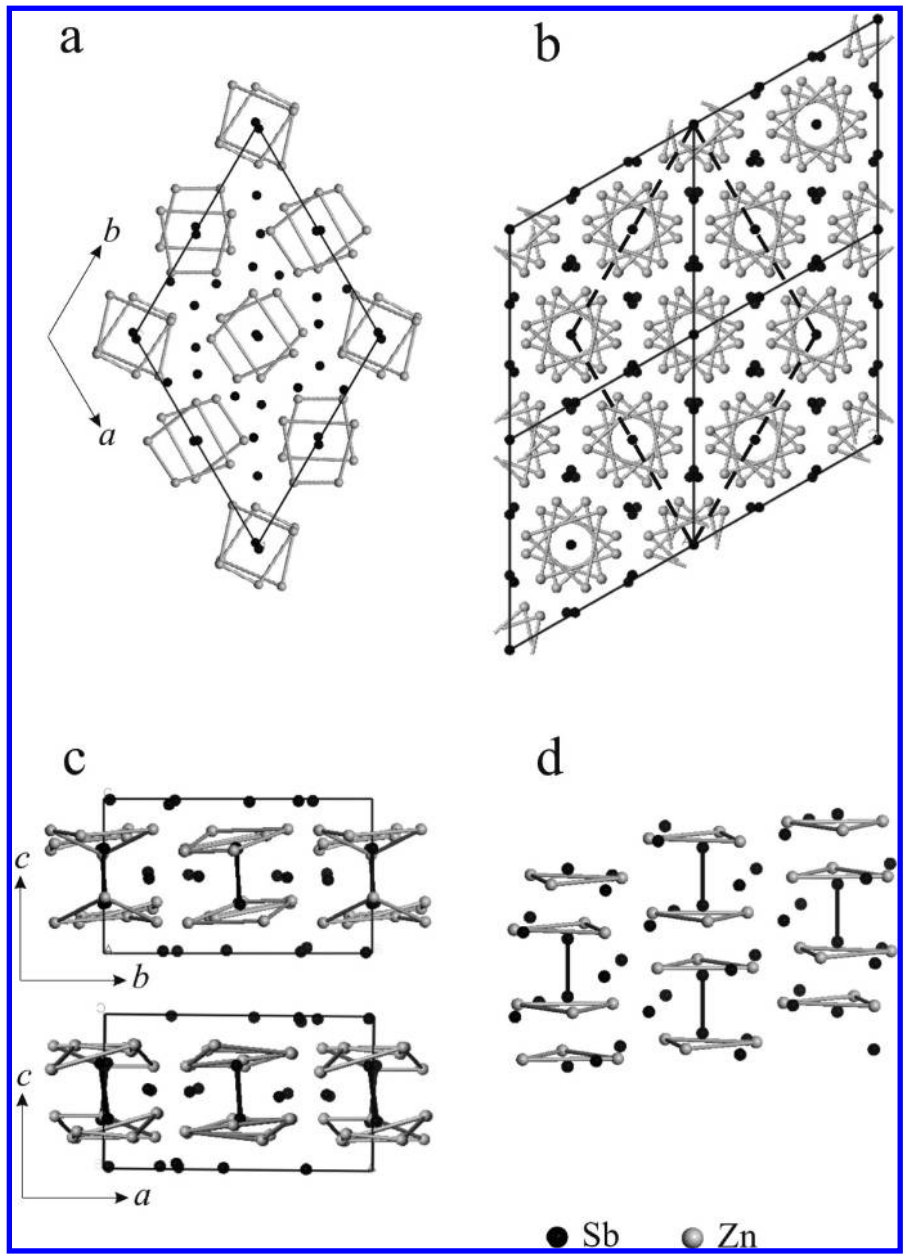

Figure 7. Relation between the crystal structure of $Zn_{1+\delta}Sb$ and $Zn_{13}Sb_{10}$.[13] (a) [001] view of the structure solved in the previous work; (b) [001] view of $Zn_{13}Sb_{10}$; (c) coordination motives of the found structure; (d) coordination motives of $Zn_{13}Sb_{10}$.

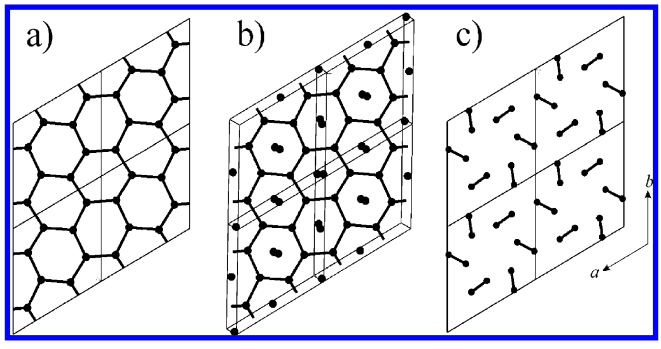

Figure 8. Arrangement of different Sb species in $Zn_{1+\delta}Sb$. (a) Hexagonal arrangement of Sb^{3-}; (b) $(Sb_2)^{4-}$ dumbbells orthogonal to the (001) plane; (c) windmill arranged $(Sb_2)^{4-}$ dumbbells in the (001) plane.

known structures: for the newly found structure these distances range from 2.66 to 3.07 Å, for the orthorhombic ZnSb phase range from 2.64 to 3.0 Å, and are 2.68 Å for the rhombohedral polymorph of $Zn_{13}Sb_{10}$.

All structures are related and include common motifs. Under nonequilibrium conditions, it is difficult to predict which crystalline phase forms; the output of the reaction is ruled by kinetic effects rather than the Gibbs free energy. In contrast to the solid state synthesis of nano-Zn_4Sb_3 reported by Schlecht,[29] this wet chemistry approach produces a Zn_4Sb_3 related nanophase in very short reaction times. This is due to the high collision rate of individual particles in liquid dispersion. On the other hand, this reaction triggered by nanoparticle collisions leads to a comparably broad particle size distribution and low crystallinity of the particle surfaces.

Conclusion

In conclusion, we have demonstrated a new low-temperature approach to the synthesis of atomically ordered nanocrystals

using nanoparticle precursors. By utilizing reduced nanosize metal precursors, solid−solid diffusion is not rate limiting; therefore, low reaction temperatures can be used that allow the formation of phases in the subsolidus regime. Avoiding high-temperature annealing minimizes sintering, and the crystalline nanoparticles can be redispersed in solution for high-volume applications. $Zn_{1+\delta}Sb$ could be obtained only in the presence of a large excess of Zn that was removed subsequently by mild acid treatment. Since diffusion clearly precedes nucleation in the bimetallic precursors, it is possible to synthesize ordered intermetallic nanocrystals near 200 °C without a high-temperature annealing step.

The TEM data show the presence of at least two crystalline phases. This raises the fundamental question how powerful and reliable structure determinations based on X-ray powder diffraction for nanomaterials with complex structures and mixtures really are. Further insight was obtained using high-resolution electron diffraction analysis of single nanoparticles. In all samples, we observe two crystalline phases, ZnSb and $Zn_{1+\delta}Sb$, phase segregated from the nano-Zn_4Sb_3 precursor that was obtained in the primary reaction from activated Zn and Sb nanoparticles.

X-ray powder diffraction data could be fitted in a first step to the crystallographic phases Zn_4Sb_3 and ZnSb, while they do not allow the distinction between the Zn_4Sb_3 and $Zn_{1+\delta}Sb$ phase due to the qualitity of the XRD data, the profile broadening, and the complexity of the corresponding crystal structures. Anyway, HRTEM showed immediately that most of the sample consisted of a new phase that cannot be fit inside the Zn−Sb system. A deeper insight was obtained using electron diffraction tomography of several single crystalline nanoparticles, obtaining cell parameters and space group of known ZnSb and a new $Zn_{1+\delta}Sb$ phase. Ab initio structure solutions were performed for both the phases on the basis of electron diffraction data obtained by automated diffraction tomography (ADT). Whereas for the orthorhombic ZnSb structure a rather limited nonprecessed ADT data set was sufficient to obtain a structure solution, precession electron diffraction data were necessary for the more complex phase $Zn_{1+\delta}Sb$. This new $Zn_{1+\delta}Sb$ phase crystallizes with a hexagonal pseudosymmetry in the triclinic space group *P*-1 and shows strict relations with both $Zn_{13}Sb_{10}$ and ZnSb. Remarkably, the structure was obtained by single-crystal analysis of a 50 nm particle, and the solution was achieved ab initio in one step with a fully kinematical approach. The correctness of the structure is supported by the reproducibility of the solution and the stability of Fourier and least-squares refinements.

Experimental Section

Synthesis. $ZnCl_2$ (ABCR) was first dried with thionylchloride, washed with toluene, dried in vacuum, and stored in a glovebox under N_2 atmosphere. Tetrahydrofuran was dried with $CaCl_2$ and Na/K and freshly distilled before use. Lithium triethylboronhydride Li[Et_3BH] (Aldrich, 1 M in THF, referred to as "superhydride") and $SbCl_3$ (ABCR) were used as obtained, and $SbCl_3$ was stored in a glovebox. Trioctylamine (Aldrich) was degassed and stored under Ar before use.

Zn particles were synthesized by reaction of $ZnCl_2$ with 2 equiv of the 1 M solution of "superhydride" in THF at ∼65 °C. The particles were washed several times with THF, dried in a vacuum, and stored in a glovebox. Sb particles were produced by reducing $SbCl_3$ with 3 equiv of the 1 M "superhydride" solution at room temperature. The black particles were repeatedly redispersed in THF and decanted from the solution, dried in a vacuum, and kept in a glovebox.

In a typical synthesis, nanoparticles of the nominal composition Zn_4Sb_3 were prepared by heating of Sb nanoparticles (0.275 mmol) with a 9-fold excess of Zn particles (2.475 mmol) in trioctylamine at ∼300 °C for 225 min. The resulting black product was collected by centrifugation (9000 rpm), washed with ethanol, and dried under a steady Ar flow. Excess of zinc was removed by repeated treatment of the particles with 2% acetic acid for about 10 min. The product was then washed with ethanol and dried with streaming Ar to a dry powder.

X-ray Powder Diffraction. X-ray powder diffraction data were collected with a Bruker-AXS D8-Discover diffractometer in reflection geometry equipped with a HiStar detector using graphite monochromatized Cu Kα radiation. Samples were glued on top of glass and (111) silicon substrates, respectively, using VP/VA copolymer (vinylpyrrolidone/vinylacetate). le Bail fits and Rietveld refinements were performed with TOPAS Academic V1.0[47] applying the fundamental parameter approach.

TEM and ADT. For TEM investigations, the sample was suspended in ethanol and sprayed onto a carbon-coated copper grid using the sonifier described in ref 35. The TEM work was carried out with a Tecnai F30 S-TWIN transmission electron microscope equipped with a field emission gun working at 300 kV. High-resolution (HR-) TEM and electron diffraction patterns were acquired with a CCD camera (14-bit GATAN 794MSC). EDX spectra were recorded in STEM mode and quantified in Emispec ESVision software.

ADT data acquisition was performed with a FISCHIONE tomography holder, using the ADT acquisition module described in ref 30. STEM images and diffraction patterns were collected using a mild illumination setting resulting in an electron dose rate of 10−15 e/Å^{2}s. STEM images were collected by a FISCHIONE high angular annular dark field detector (HAADF). Nano electron diffraction was performed employing a 10 μm C2 condenser aperture with a 50 nm beam on the sample. ADT data were collected in standard ED as well as PED mode in steps of 1°.

PED was performed using the SpinningStar unit NanoMEGAS.[48] The precession angle was kept at 0.6°, and the precession frequency was 100 Hz.

The self-developed ADAP package[31] written in Matlab was used for the data processing, including 3D diffraction volume reconstruction, automated cell parameter determination, and intensity integration procedures. For the visualization and validation of the 3D data sets, we used the newly developed ADT-3D software package programmed in C++.[49] The ab initio structure solution was performed by direct methods implemented in SIR2008, included in the package Il Milione.[41] The structure refinement was performed using SHELXL97.[42]

Acknowledgment. This work was supported by the Deutsche Forschungsgemeinschaft (DFG) within the priority program 1386 *Nanostrukturierte Thermoelektrika: Theorie, Modellsysteme und kontrollierte Synthese* and the Deutsche Forschungsgemeinschaft (DE 412/37-1). C.S.B. is a recipient of a fellowship from MATCOR, the Graduate School of Excellence of the State of Rhineland-Palatinate. We acknowledge the help of Mr. G. Glasser with the SEM and support from the Materials Science Center (MWFZ) in Mainz. We thank Ulrich Heil, Sebastian Schlitt, and Prof. Elmar Schömer from the Institute of Computer Science, Johannes Gutenberg-University of Mainz, for cooperation evolving the ADT-3D

(47) Coelho, A. *TOPAS Academic V1.0*; Coelho Software: Brisbane, Australia, 2004.
(48) *NanoMEGAS, Advanced Tools for Electron Diffraction*; NanoMEGAS: Brussels, Belgium, 2004.
(49) Heil, U.; Schlitt, S.; Kolb, U.; Gorelik, T.; Mugnaioli, E.; Schömer, E. *ADT-3D. A software package for ADT data visualizing and processing*, Cooperation with the Institute of Computer Science, Johannes Gutenberg University of Mainz: Mainz, Germany, 2009.

software package used for 3d data processing and visualization. Dedicated to Prof. Robert Schöllhorn on the occasion of his 75th birthday.

Supporting Information Available: (1) ^{1}H NMR data of Sb, (2) DTA data of the $Zn_{1+x}Sb$ sample showing the exothermic decomposition of the $Zn_{1+\delta}$ phase (~200 °C) and the endothermic melting of Zn (~410 °C), (3) X-ray diffraction and le Bail fits of the raw product, (4) SEM overview image of $Zn_{1+x}Sb$, (5) HRTEM image of a $Zn_{1+\delta}Sb$ nanoparticle, (6) EDX data for $Zn_{1+\delta}Sb$, (7) projection of the full 3D reciprocal space for the orthorhombic phase I, (8) plot of the ZnSb structure, (9) atomic coordinates of Zn and Sb for ZnSb obtained using nonprecessed electron diffraction data, and (10) atomic coordinates of Zn and Sb for $Zn_{1+\delta}Sb$. This material is available free of charge via the Internet at http://pubs.acs.org.

JA1035122